J Petrol Explor Prod Technol (2012) 2:15–27
DOI 10.1007/s13202-011-0017-3

ORIGINAL PAPER - PRODUCTION ENGINEERING

Study of constant-pressure production characteristics of class 1 methane hydrate reservoirs

Suntichai Silpngarmlert · Luis F. Ayala H. · Turgay Ertekin

Received: 3 October 2011 / Accepted: 23 December 2011 / Published online: 26 January 2012

Abstract A three-dimensional, compositional, multiphase flow simulator for methane-hydrate reservoirs is developed in this study. It is used to study the production characteristics of class 1 methane-hydrate reservoirs. The effects of well-completion location, well spacing, and production schedule on gas production efficiency are also examined. All simulation studies in this work implement a constant bottom-hole pressure (at 14.7 psia) as a production scheme for exploring maximum production capacity from the reservoir. The simulation study shows that the presence of gas hydrate on top of a conventional gas reservoir can dramatically improve gas productivity. Unlike conventional gas reservoirs, the water production rate of gas-hydrate reservoirs increases with time (when a constant bottom-hole pressure is implemented as a production scheme). Moreover, it shows that moving well-completion location in free-gas zone (in relation to the movement of the interface between free-gas and hydrate zones) provides better production performance and the best completion location is in the middle of free gas zone. As expected, the results also show that smaller well spacing yields higher gas production. However, for a particular system used in this work, it does not show substantial improvement of production efficiency. For a multiple-well system, the simulation results indicate that production efficiency can be improved by putting the wells on production at different times.

S. Silpngarmlert · L. F. Ayala H. (✉) · T. Ertekin
Department of Energy and Mineral Engineering,
The Pennsylvania State University, 109 Hosler Building,
University Park, PA 16802-5001, USA
e-mail: lfay@psu.edu

Keywords Natural gas-hydrates · Depressurization · Mathematical modeling · Development

List of symbols

A	Flow area (ft^2)
a	Capillary pressure shape parameter (–)
b	Capillary pressure shape parameter (–)
c	Capillary pressure exponent (–)
n	Permeability-porosity or relative permeability correlation parameter (–)
h	Phase specific enthalpy (BTU/lb_m)
K_h	Thermal conductivity of formation (BTU/ft-day-F)
K	Permeability (perms)
k_r	Relative permeability (–)
N_m	Number of methane molecules in hydrate structure (–)
N_w	Number of water molecules in hydrate structure (–)
P_e	Gas entry pressure (psia)
Q_{dis}	Heat sink/source for hydrate dissociation (BTU/day)
Q_E	External heat sink/source (BTU/day)
Q_{fus}	Heat sink/souce for ice fusion (BTU/day)
Q_m	Methane molar sink/source (lbmol/day)
Q_w	Water molar sink/source (lbmol/day)
S	Phase saturation (–)
S_{ir}	Irreducible saturation (–)
T	Temperature (F)
v	Phase velocity (ft/day)
V_b	Gridblock bulk volume (ft^3)
x_m	Mole fraction of methane in aqueous phase (–)
y_m	Mole fraction of methane in free gas phase (–)

Greek

ρ	Mass density (lb_m/ft^3)
$\bar{\rho}$	Molar density (lbmol/ft^3)
ϕ	Porosity including ice or hydrate phase in the pore space (–)

ϕ_c	Critical porosity (–)
ϕ_0	Ice- and hydrate-free rock porosity (–)
θ_{dry}	Dry thermal conductivity (BTU/ft-day-F)
θ_{wet}	Wet thermal conductivity (BTU/ft-day-F)
θ_I	Ice thermal conductivity (BTU/ft-day-F)
Φ	Hubbert's potential (psia)
μ	Fluid viscosity (cp)

Subscripts

x, y, z	Cartesian coordinates
g, a, H, i, s	Gas, aqueous, hydrate, ice, solid (hydrate + ice) phases
m, w	Methane, water components

Introduction

Gas hydrates are drawing worldwide attention as an unconventional source of energy because of its vast availability. It is estimated that the amount of natural gas being trapped in gas hydrate deposits varies between 10^{15} and 10^{19} std. m^3 (3.5×10^4 to 3.5×10^{10} trillion std. ft^3) and is believed to be the major organic carbon reserve on Earth (Mahajan et al. 2007). It has been also estimated that the current world energy consumption could be sustained for about 200 years by recovering just 15% of the estimated gas hydrate resource (Makogon et al. 2007). The feasibility of gas production from class 1 methane-hydrate reservoirs has been examined by several researchers (e.g., Holder and Angert 1982; Burshears et al. 1986; Moridis 2003; Pooladi-Darvish 2004; Sun et al. 2005; Moridis et al. 2007, 2009, 2011; Mahajan et al. 2007). The simulation results from previous studies showed the good potential for gas production from class 1 gas-hydrate accumulations. However, none of the previous studies focused on the effects of a variety of production parameters on the production performance of gas hydrate system and their implications for reservoir development. In this work, the effects of different production parameters such as well-completion location, well spacing, and production schedule on the production efficiency are investigated to gain more understanding about gas production from class 1 gas-hydrate reservoirs. For the analysis, a three-dimensional, compositional, multiphase flow simulator for methane-hydrate reservoirs recently developed has been implemented (Silpngarmlert et al. 2012).

Governing equations

In a compositional hydrate reservoir simulator, material balance equations are written for methane and water components as follows:

Methane

$$\frac{\partial}{\partial x}\left[y_m\bar{\rho}_g\frac{A_xk_xk_{rg}}{\mu_g}\left(\frac{\partial\Phi_g}{\partial x}\right)+x_m\bar{\rho}_a\frac{A_xk_xk_{ra}}{\mu_a}\left(\frac{\partial\Phi_a}{\partial x}\right)\right]\Delta x + \frac{\partial}{\partial y}\left[y_m\bar{\rho}_g\frac{A_yk_yk_{rg}}{\mu_g}\left(\frac{\partial\Phi_g}{\partial y}\right)+x_m\bar{\rho}_a\frac{A_yk_yk_{ra}}{\mu_a}\left(\frac{\partial\Phi_a}{\partial y}\right)\right]\Delta y + \frac{\partial}{\partial z}\left[y_m\bar{\rho}_g\frac{A_zk_zk_{rg}}{\mu_g}\left(\frac{\partial\Phi_g}{\partial z}\right)+x_m\bar{\rho}_a\frac{A_zk_zk_{ra}}{\mu_a}\left(\frac{\partial\Phi_a}{\partial z}\right)\right]\Delta z+\frac{Q_m}{5.615} = \left(\frac{V_b}{5.615}\right)\frac{\partial}{\partial t}\left(y_m\phi S_g\bar{\rho}_g+x_m\phi S_a\bar{\rho}_a+N_m\phi S_H\bar{\rho}_H\right) \quad (1)$$

Water

$$\frac{\partial}{\partial x}\left[(1-y_m)\bar{\rho}_g\frac{A_xk_xk_{rg}}{\mu_g}\left(\frac{\partial\Phi_g}{\partial x}\right)+(1-x_m)\bar{\rho}_a\frac{A_xk_xk_{ra}}{\mu_a}\left(\frac{\partial\Phi_a}{\partial x}\right)\right]\Delta x + \frac{\partial}{\partial y}\left[(1-y_m)\bar{\rho}_g\frac{A_yk_yk_{rg}}{\mu_g}\left(\frac{\partial\Phi_g}{\partial y}\right)+(1-x_m)\bar{\rho}_a\frac{A_yk_yk_{ra}}{\mu_a}\left(\frac{\partial\Phi_a}{\partial y}\right)\right]\Delta y + \frac{\partial}{\partial z}\left[(1-y_m)\bar{\rho}_g\frac{A_zk_zk_{rg}}{\mu_g}\left(\frac{\partial\Phi_g}{\partial z}\right)+(1-x_m)\bar{\rho}_a\frac{A_zk_zk_{ra}}{\mu_a}\left(\frac{\partial\Phi_a}{\partial z}\right)\right]\Delta z + \frac{Q_w}{5.615}=\left(\frac{V_b}{5.615}\right)\frac{\partial}{\partial t}\left((1-y_m)\phi S_g\bar{\rho}_g+(1-x_m)\phi S_a\bar{\rho}_a + \phi S_I\bar{\rho}_I+N_w\phi S_H\bar{\rho}_H\right) \quad (2)$$

Since hydrate dissociation is an endothermic reaction, it is necessary to incorporate an energy balance equation into the model. Heat transfer through both conduction and convection is taken into account in this work. The energy balance equation used in this work can be written as

$$\frac{\partial}{\partial t}\left\{\phi\left(\rho_gS_gh_g\right)+\phi(\rho_aS_ah_a)+\phi(\rho_HS_Hh_H)+(1-\phi)(\rho_rh_r)\right\} = \nabla\cdot(K_h\nabla T)-\nabla\cdot\left[\rho_gv_gh_g+\rho_av_ah_a\right]+\frac{(Q_E-Q_{dis}+Q_{fus})}{V_b} \quad (3)$$

The finite difference approximation is used for the discretization of the three governing equations to obtain a system of algebraic equations. Because of the complex nature of hydrate accumulation and dissociation processes, several assumptions are made to simplify the model. The important assumptions of this work are (a) geomechanics effects are ignored, (b) only aqueous and free-gas phases are mobile, (c) no fluid flows across system boundaries, (d) shale layers are assumed to be impermeable but they allow heat transfer between surroundings and the reservoir, (e) heat transfer across system boundaries along the x- and y-directions is negligible (compared with heat transfer along the vertical direction) because reservoir thickness is assumed to be quite thin comparing with its drainage area, (f) ideal liquid behavior is assumed for aqueous phase, (g) hydrate formation and dissociation are assumed to be instantaneous, and (h) the current state of this work simply focuses on the

formation and it does not take into consideration any processes within the wellbore domain.

One of the major challenges in hydrate modeling is to properly capture all the important mechanisms associated with hydrate dissociation. Even though the governing equations stated above can be straightforwardly derived from a compositional mass balance on each of the species, most of the terms involved in them are highly non-linear and interdependent. The work of Silpngarmlert et al. (2012) explains in detail each of the assumptions and property dependencies built into this formulation. For example, the solid phases (hydrate and ice) in the porous medium are considered typically immobile in hydrate modeling and only aqueous and free gas phases are allowed to flow through the porous medium. Thus, the presence of solid phase changes porosity and absolute permeability of porous rock. In the case that the data of rock permeability at various hydrate and ice saturations are not available, based on "tube-in-series" model of pore space, the change of rock permeability due to the change in hydrate saturation can be calculated from the following correlation (Verma et al. 1985; Moridis et al. 2008):

$$\frac{k}{k_0} = \left(\frac{\phi - \phi_c}{\phi_0 - \phi_c}\right)^n \tag{4}$$

where

ϕ_c	Critical porosity,
ϕ_0	Rock porosity (ice- and hydrate-free porosity),
k_0	Permeability at ϕ_0,
N	Correlation parameter,
ϕ	Rock porosity (with ice or hydrate phase in the pore space),
K	Permeability at ϕ

For relative permeability calculation purposes, the immobile solid phases (hydrate and ice phases) were treated as parts of porous rock, and normalized aqueous and free gas saturations were used in relative permeability calculation (see Eq. 5).

$$\begin{aligned} k_{ra} &= \left[\left(S_a^* - S_{ira}\right)/\left(1 - S_{ira}\right)\right]^{n_a} \\ k_{rg} &= \left[\left(S_g^* - S_{irg}\right)/\left(1 - S_{ira}\right)\right]^{n_g} \\ S_a^* &= S_a/\left(S_a + S_g\right), S_g^* = S_g/\left(S_a + S_g\right) \end{aligned} \tag{5}$$

where

S_a	Aqueous phase saturation,
S_g	Free gas phase saturation,
S_{ira}	Irreducible water saturation,
S_{irg}	Critical gas saturation,
n_a and n_g	Exponential parameters.

Capillary pressures between aqueous and free-gas phases are expected to be a strong function of hydrate saturation because the formation of hydrates reduces pore size diameter of porous media, which results in an increase of capillary pressure. Moridis et al. (2008) proposed modeling this relationship using the following expression, which is implemented in this work (see Eq. 6):

$$P_{cap}(S_H, S_{aA}) = H(S_H) \cdot F \cdot P_e \cdot (S_{aA})^c \tag{6}$$

where

P_{cap}	Gas entry pressure,
P_e	Gas entry pressure,
C	A negative exponent ($\lvert c \rvert < 1$),
S_{aA}	$(S_A - S_{irA})/(1 - S_{irA})$
F	erf [60 $(1 - S_{aA})$]
S_{irA}	Irreducible water saturation,
S_A	Aqueous phase saturation,
$H\ (S_H)$	$1 + B_x(a,b,S_S)$
$B_x(a,b,S_S)$	The incomplete beta function,
S_H	Hydrate saturation,
S_s	Solid (hydrate and/or ice) saturation, and
a and b	Shape parameters

Because the thermal conductivities of different phases are different, the change of saturations can significantly affect the thermal conductivity of the system. In this work, the extension of the model by Somerton (1973) proposed by Moridis et al. (2005) is used because it provides better predictions than the commonly used linear model based on the saturation-weighted contributions of the phases and rock (see Eq. 7).

$$K_h = \theta_{dry} + \left(S_a^{0.5} + S_H^{0.5}\right)\left(\theta_{wet} - \theta_{dry}\right) + \varphi S_I \theta_I \tag{7}$$

where

θ_{dry}	Dry thermal conductivity,
θ_{wet}	Wet thermal conductivity,
θ_I	Thermal conductivity of ice,
S_a, S_H, S_I	Saturations of aqueous, hydrate, and ice phases, respectively.

The empirical correlation proposed by Moridis and Collett (2003) is used for calculating dissociation pressure of methane hydrates based on experimental data and a linear interpolation technique is used to calculate the aqueous phase density and viscosity at prevailing temperature using the water data published by Perry (1997). Compressibility factors and enthalpies of the free-gas phase are calculated using the Peng–Robinson equation of state (Peng and Robinson 1976). The Lee et al. (1966) correlation is used to determine the free-gas phase viscosity. Peaceman's wellbore model is used in this work for the representation of wellbore fluid withdrawal (Peaceman 1983).

Numerical representation and validation

As explained in detail in Silpngarmlert et al. (2012), the Newton–Raphson method is used for the linearization of

the fully implicit governing equations. All the parameters are updated at every iteration. The Generalized Minimal Residual Method (GMRES) is used for the solution of the resulting simultaneous system of algebraic equations. The class 1 hydrate reservoir structure presented by Burshears et al. (1986) was used in this work as a reference system for validation purposes (Silpngarmlert et al. 2012). This base or reference system has a 50-ft-thick Hydrate Bearing Layer (HBL) in the upper part and 50-ft-thick free gas and water zone underneath the HBL, as indicated in Fig. 1. There are about 45-ft-thick shale layers above the HBL and below the free-gas zone. The pressure at the bottom of the HBL is about 3,000 psia. Reservoir properties are summarized in Table 1. This reservoir pressure is quite high but it is not unfeasible. According to the geological data of gas hydrate deposit in TigerShark area in the Gulf of Mexico (Boswell et al. 2009), the average reservoir pressure is above 4,500 psia (approximated from hydrostatic pressure). For the discretized model, a 3D (x,y,z) representation is implemented using gridblock sizes of 100 ft × 100 ft × 10 ft. For the particular case of this reference case the number of equations that needs to be solved at each iteration is about 15,500 equations for a drainage area of 73.38 acres. Hydrostatic and geothermal gradient values are used to estimate P–T conditions of each grid block in each zone (hydrate and free-gas zones). Simulation runs of each zone are performed separately to estimate initial conditions in each zone. The temperature at the top boundary of the top shale is adjusted to match the heat flux at the bottom of this zone to that of the top layer of the free-gas zone. After that, the two parts are combined and then a simulation run of the combined model is performed (without production) to obtain the initial conditions of the entire reservoir. There is no gas–water contact in the free-gas zone. Details about the validation of the proposed model using the described reference case are found in Silpngarmlert et al. (2012).

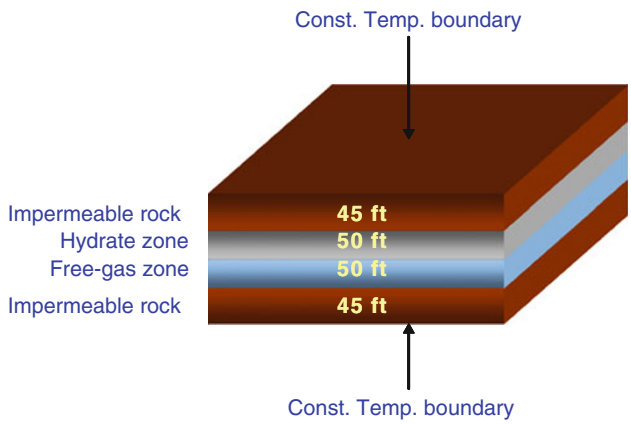

Fig. 1 Structure of the reference methane hydrate reservoir used in this study

Table 1 Reservoir properties and correlation parameters used in this study

Rock properties		Value
Rock porosity (homogeneous)		30%
Heat conductivity (wet)		1.7911 BTU/h-ft-°F (3.1 W/m–K)
Heat conductivity (dry)		0.2889 BTU/h-ft-°F (0.5 W/m–K)
Rock density (homogeneous)		162.31 lb/ft^3 (2,600 kg/m^3)
Rock permeability		1,000 mD (1.0×10^{-12} m^2)
Specific heat of rock		0.22 BTU/lb-°F (0.92 kJ/kg-K)
Properties	**Parameters**	**Value**
Permeability	n	3
	$\cup_0$	0.3
	$\cup_c$	0.07
	k_0	1,000 mD
Capillary pressure	S_{wirr}	0.25
	p_e	2.248 psia (15,500 Pa)
	c	−0.65
	a	2.1
	b	2.2

Simulation study

In the present study, the effects of some production parameters on gas production performance are examined. The reservoir properties and all parameter values used in this study are summarized in Table 1. The model implements parameter switching method to handle phase change in each grid block in the system. The unknowns in each grid blocks are determined from the phase presented in the grid blocks. Table 2 summarizes the unknowns for each expected phase combinations in this simulation study. In order to explore maximum production capacity of a given well, production wells in all simulation cases are operated with constant bottom-hole pressure (BHP) at 14.7 psia. Note that the 14.7 psia case shows the maximum production that could be expected. However, comparison of cumulative gas and productions at 14.7 and 500 psia of one simulation case was provided (Fig. 14).

Study of production characteristics

Production characteristics of a class 1 methane hydrate reservoir are compared with the production characteristics of a conventional gas reservoir. The main objective of this simulation study is to compare the production characteristics between conventional gas and gas-hydrate reservoirs.

Table 2 Set of unknowns for each expected phase combination

Case	Phases	Principal unknowns
1	H + A	T, P_a, S_H
2	H + G	T, P_g, S_H
3	G + A	T, P_g, S_a
4	H + A + G	T, S_g, S_a

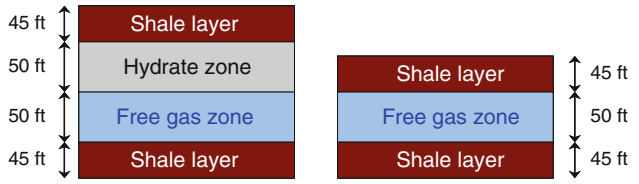

(a) Methane-hydrate reservoir **(b)** Conventional gas reservoir

Fig. 2 Structures of the methane hydrate and conventional gas reservoirs

Table 3 Methane-hydrate and conventional gas reservoir properties

Properties	Methane-hydrate reservoir	Conventional gas reservoir
Reservoir thickness	100 ft	50 ft
Gas zone thickness	50 ft	50 ft
Hydrate zone thickness	50 ft	0 ft
Reservoir porosity	30%	30%
Reservoir permeability	44 mD	44 mD
Initial pressure	3,000 psia	3,000 psia
Intial temperature	65.8°F	65.8°F
Gas composition	100% CH_4	100% CH_4
Thermal conductivity	1.56 BTU/ft-Hr-°F	1.56 BTU/ft-Hr-°F

Figure 2 shows the structures of the two reservoirs used in this simulation study. The purposes of this simulation study are to compare the production characteristics of the two systems and to determine whether a presence of gas-hydrate cap on top of a conventional gas reservoir can significantly increase gas productivity. There are 45-ft-thick shale layers at the top and bottom of the reservoir in both cases. The reservoir properties of the two systems are summarized in Table 3. The production wells of the two reservoirs are completed just in the middle of the free gas-zone, and they are operated with a constant BHP at 14.7 psia. The lengths of the well completion in both cases are 10 ft (Table 4).

Figure 3 shows the gas production rate prediction for the two systems under consideration. The gas production rate from the conventional gas reservoir drops more rapidly than that from the gas-hydrate reservoir. This is because released gas from hydrate dissociation in gas-hydrate system helps maintaining reservoir pressure. Accordingly, reservoir pressure in the conventional gas reservoir drops faster resulting in the more rapid decrease of gas production rate in the conventional gas reservoir. Figure 4 indicates the significant improvement of cumulative gas

Table 4 Cumulative gas productions of three different well-spacing systems

Well spacing (acres)	Number of wells	Gas production (MMSCF)	Improvement (%)
22.95	20	74,365	15.34
45	10	69,891	8.4
74.38*	6	64,474	0

* Reference case

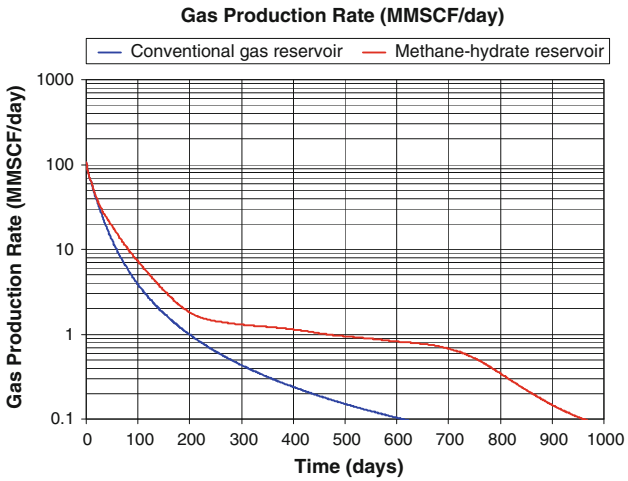

Fig. 3 Gas production rates from methane-hydrate and conventional gas reservoirs

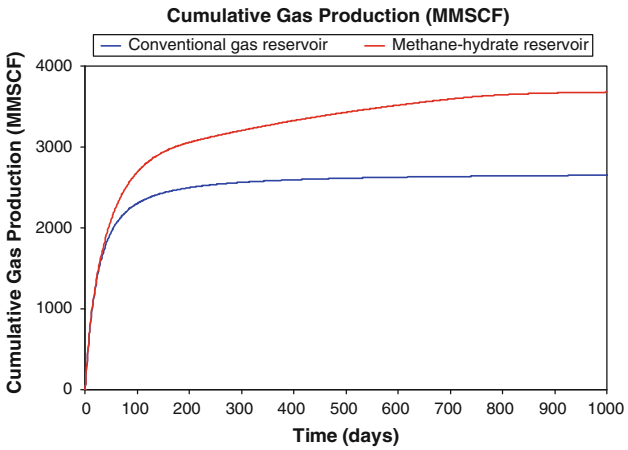

Fig. 4 Cumulative gas productions of methane-hydrate and conventional gas reservoirs

production (increases by about 38.74% at 1,000 days) when there is a gas hydrate cap on top of the conventional gas reservoir. However, it does not imply that the gas-hydrate reservoir yields higher gas recovery because there is more gas available in the methane-hydrate reservoir (free gas in the free-gas zone plus gas in methane-hydrate crystal), since the two systems have the same amount of free gas at initial condition. It could be roughly said that additional gas production from gas-hydrate reservoir comes from released gas from hydrate dissociation.

Figure 5 shows different water production characteristics between methane-hydrate and conventional gas reservoirs. Water production rate for the gas hydrate reservoir substantially increases with time, whereas the water production rate for the conventional gas reservoir decreases with time. This is due to the substantially increase of aqueous phase saturation around the well in the gas-hydrate system, whereas aqueous phase saturation around the well in the conventional gas reservoir does not dramatically change (see Fig. 6). Figures 6 and 7 show the consistency between water saturation at the well block (formation around the well) and water production rate profiles. The increase of water saturation around the well increases the mobility of aqueous phase resulting in the increase of water production rate. Note that released water from hydrate dissociation in the upper part of the reservoir flows down to free gas zone resulting in significant increase of water saturation around the completion zone as shown in Fig. 7.

Based on the aforementioned observation, it could be concluded that

- The presence of gas hydrate on top of a conventional gas reservoir can significantly improve gas productivity.
- In gas-hydrate systems, while gas production rate decreases with time, water production rate increases with time (when a constant BHP is used as a production scheme).

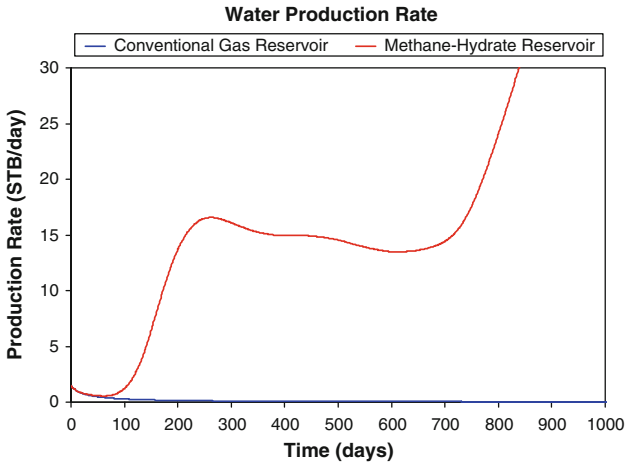

Fig. 5 Water production rates of conventional and methane-hydrate reservoirs

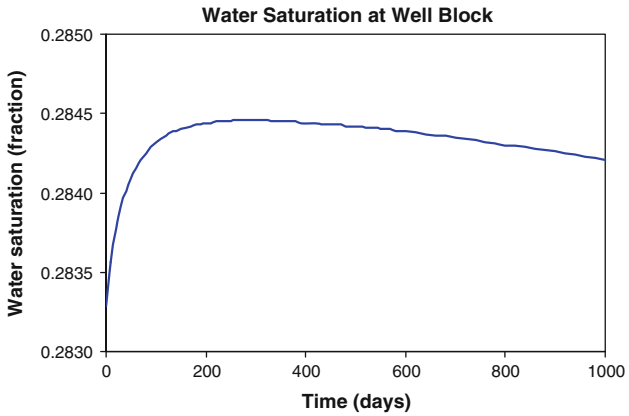

(a) Conventional gas reservoir

Fig. 6 Water saturation—conventional system

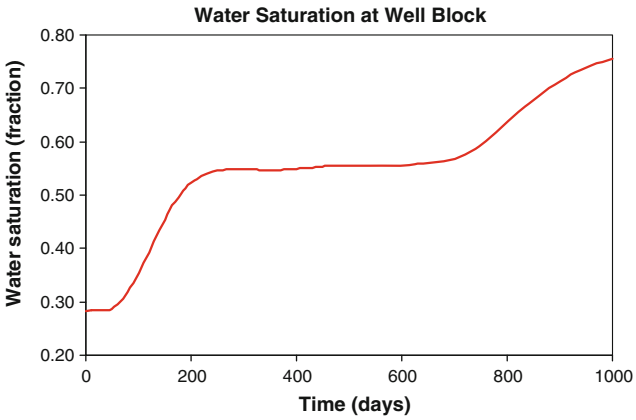

(b) methane-hydrate reservoir

Fig. 7 Water saturation—hydrate system

Effects of well-completion location

In this case, the effect of four different well-completion locations shown in Fig. 8 on production performance is examined. The length of well completion is 10 ft in all cases. Again, the production wells are operated with a constant BHP at 14.7 psia. The well-completion zone of the wells for Cases 1, 2, and 3 are located at the middle, top, and bottom of the initial free-gas zone, respectively. In Case 4, the well is completed inside the hydrate zone (just above the bottom of hydrate zone). Note that the completion location in each case does not change for the entire simulation even though the location of the interface between hydrate and free-gas zones changes with time.

The gas production rate and cumulative gas productions of these four cases are shown in Figs. 9 and 10,

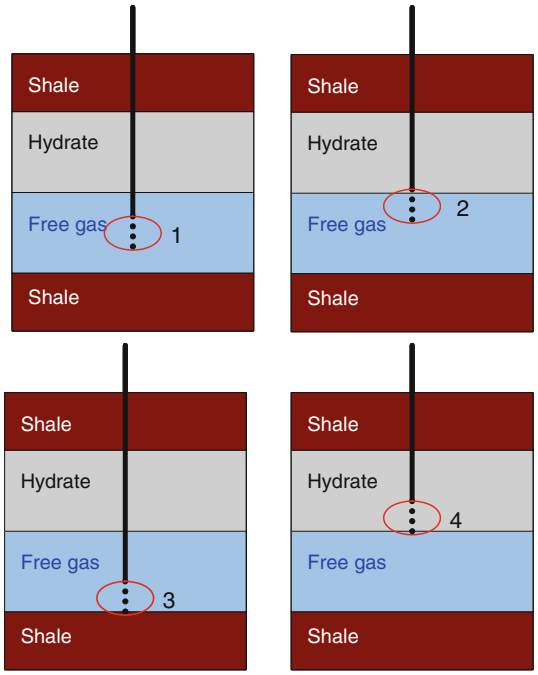

Fig. 8 Well-completion locations used in this study

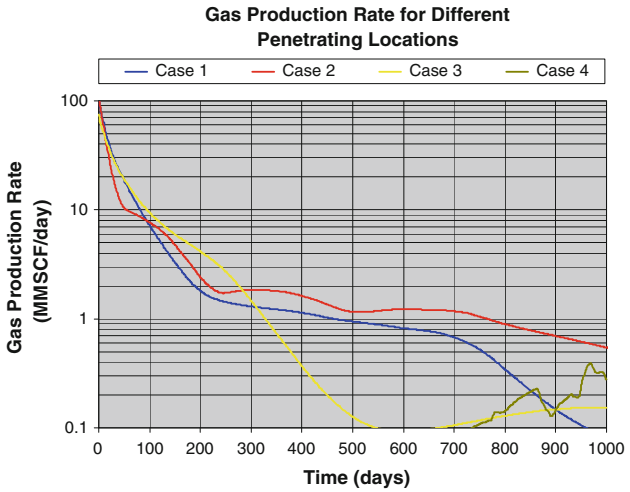

Fig. 9 Gas production rates of different well-completion location cases

respectively. Case 4 yields the lowest gas production because hydrate dissociation rate in this case is very small. Since permeability in the hydrate zone is very small (almost impermeable) which is caused by the presence of gas hydrate in pore space, just small amount of movable fluids (initially almost water is produced) around the completion zone flows toward the well. As a result, pressure in the region around the well slightly drops. Accordingly, very little fluids in the regions above and below the completion zone flow toward the well during early production period. However, as one can see some gas

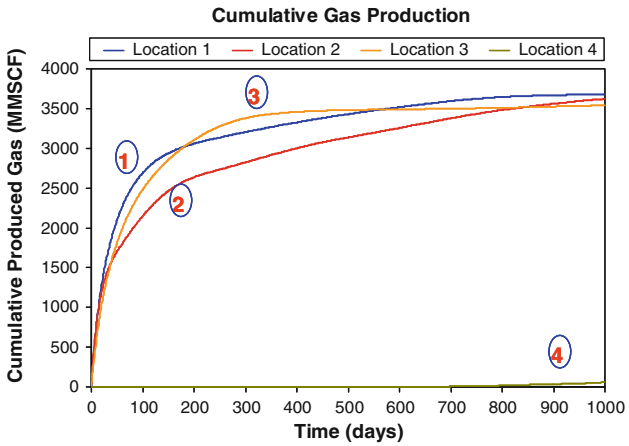

Fig. 10 Cumulative gas productions of different well-completion location cases

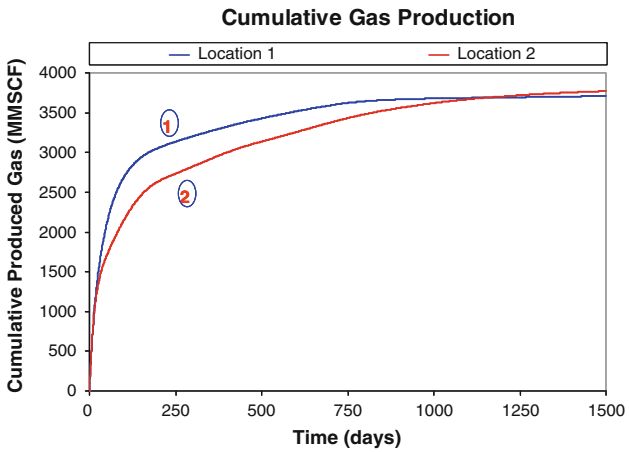

Fig. 11 Cumulative gas productions of Case 1 and Case 2

produced at late time (after 900 days), this indicates that hydrate dissociation has been taking place. As a result, effective permeability around the completion zone increases with time due to the decrease of hydrate saturation in this zone and fluids in the regions above and below the completion zone move toward the well more easily. At the end of 1,000 days, Case 1 yields the highest gas production. However, cumulative gas production from Case 2 becomes a bit higher than that of Case 1 at the end of 1,500 days (see Fig. 11).

The simulation results shown in Figs. 9, 10, 11 are the results for the cases that well-completion locations do not change for the entire simulation period. In the following simulation exercise, well-completion locations are moving in relation to the movement of the interface between methane-hydrate and free-gas zones. The movement of the interface between hydrate and free-gas zones is caused by hydrate dissociation of gas hydrate. Even though hydrate dissociation takes place not only at the interface but also

inside hydrate zone, hydration dissociation taking place at the interface is faster due to higher pressure drop and higher temperature at the interface. The simulation results show the appearance of secondary hydrate dissociation at the top of hydrate zone resulting from heat transfer from the shale layer to the hydrate zone which agrees with the Moridis et al. (2008) observation. In this study, the effects of moving well-completion locations of Cases 1 and 2 (the best two cases from previous simulation exercise) are examined.

Figures 12 and 13 show the cumulative gas and water productions of these two cases, respectively. Case 1 (well-completion location is in the middle of free-gas zone) provides better production efficiency because it yields higher gas production and lower water production than Case 2. By inspection of the gas and water production plots corresponding to the moving completion versus the fixed completion location of Case 1, it is clear that production efficiency could be improved by moving well-completion location in relation with the movement of the interface between hydrate and free-gas zones.

Figure 14 compares cumulative gas and productions from Case 1 at two different BHP pressures: 14.7 and 500 psia. Cumulative gas and water productions in the 14.7 psia case are higher as anticipated because more gas and water released to the completion zone.

Effects of well spacing/well-drainage area

In this simulation exercise, the effects of well spacing or well drainage area on the gas production efficiency are investigated. In this case, gas production performances of three different well-spacing systems (22.95, 45.00, and 74.38 acres) for a 450-acre class 1 methane-hydrate reservoir are compared. Figure 15 shows gas production rate (per one well) from these three well-spacing systems, whereas Fig. 16 shows total cumulative gas production from the 450-acre reservoir. Note that total numbers of wells in the three cases are different, i.e., the smaller well-spacing system has more production wells. Figure 17 shows percent of methane hydrate which has dissociated

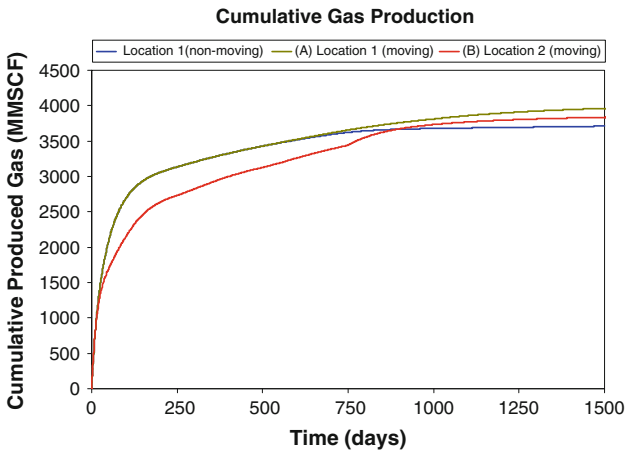

Fig. 12 Cumulative gas production—moving completion location cases

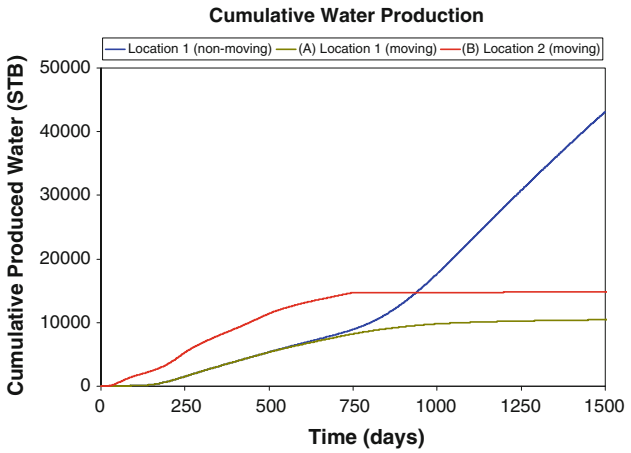

Fig. 13 Cumulative water productions—moving completion location cases

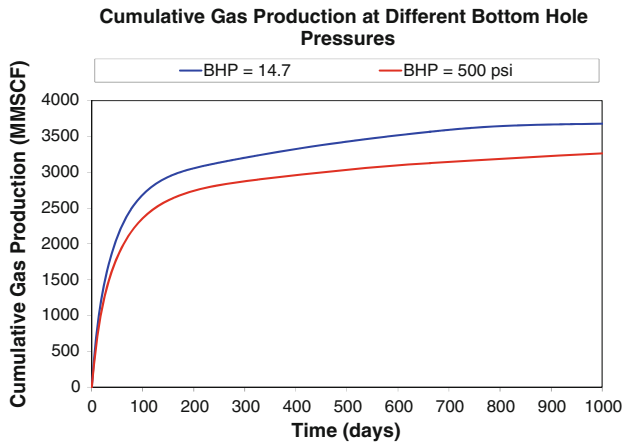

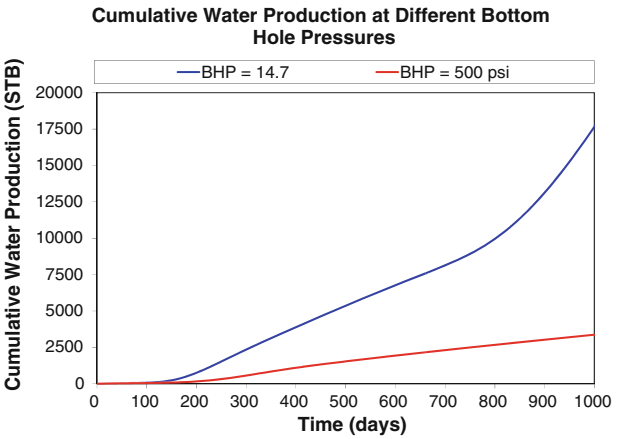

Fig. 14 Cumulative gas and water productions in Case 1 at 14.7 psi and 500 psi BHP

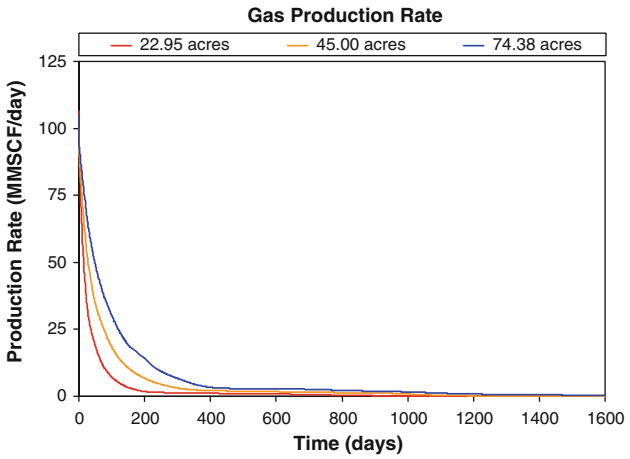

Fig. 15 Gas production rates (one well) from different well-spacing systems

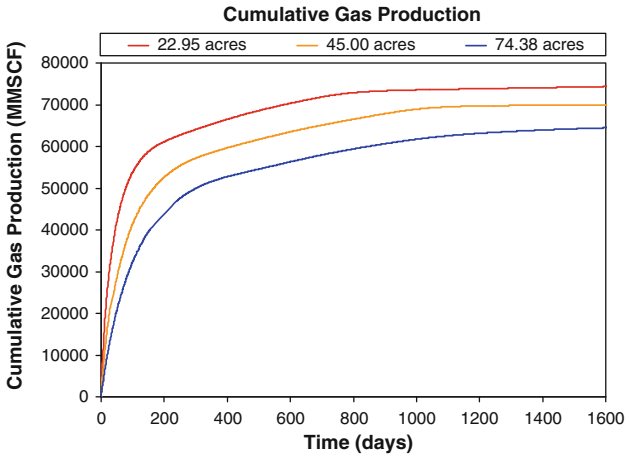

Fig. 16 Cumulative gas production from different well-spacing systems (450-acre reservoir)

during the production period. Some of the released gas from hydrate dissociation may not be produced such as the gas released from hydrate dissociation taking place at the top of hydrate zone. The released gas is not produced because the completion zone is located in the lower part of the reservoir.

As expected, the simulation results show that smaller well spacing system yields higher gas production, and it can dissociate gas hydrate in the system more rapidly. The numbers next to the curves in Fig. 17 indicate the time needed for dissociating 100% of methane hydrate in the system. Cumulative gas productions at 1,600 days of these three systems are summarized in Table 3. For this particular system, cumulative gas production increases by about 8.4% when the well-spacing decreases from 74.38 to 45.00 acres and the gas production increases just by 15.34% when the well-spacing decreases from 74.38 to 22.98 acres. The average reservoir pressure (especially in

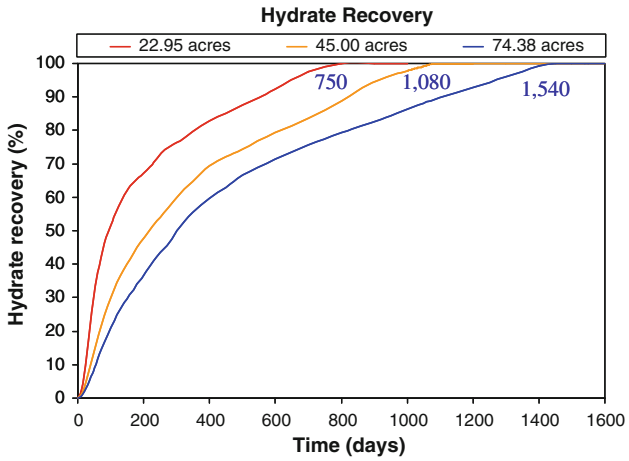

Fig. 17 Percent of methane-hydrate dissociations in different well-spacing systems

the free-gas zone) in a smaller well-spacing system drop more rapidly than that in a larger well-spacing system. Consequently, hydrate dissociation takes place more rapidly (especially at the interface between free-gas and hydrate zone) than a larger well-spacing system. Since hydrate dissociation is an endothermic reaction, faster hydrate dissociation causes more rapid temperature decrease within the hydrate zone. As a result, temperature gradient between hydrate zone and cap rock increases which will introduce more heat transfer from the cap rock to the system. Note that the initial temperature in the hydrate zone is higher than the initial temperature in the cap rock. But after hydrate dissociation taking place for certain period of time, the temperature of the hydrate zone becomes lower than the temperature in the cap rock. However, the results do not show substantial increase of gas production when the well spacing decreases. This is because the heat transfer from the cap rock to hydrate zone induces mostly hydrate dissociation at the top part of hydrate zone and the released gas still remains in that region. More produced gas comes from higher dissociation rate at the interface between hydrate and free gas zones which is caused by higher pressure reduction rate in the free gas zone in smaller well-spacing systems.

The conclusion which can be drawn from this numerical simulation exercise is that, for the specific case of gas hydrate reservoirs of class 1, smaller well-spacing system tends to yield higher gas production. However, for the particular gas hydrate system used in this study, it did not provide a substantial improvement in gas productivity.

Effects of production schedule

The production performances from a class 1 methane-hydrate reservoir with four production wells as shown in

Fig. 18 using four different production schedules are examined. All production wells are operated with constant BHP at 14.7 psia. Four different production schedules shown in Table 5 are examined. Figures 19, 20, 21, 22 show the gas production rates, cumulative gas productions, cumulative water productions, and water production rates for each production schedule, respectively. The cumulative gas production of Case (a) is lower than that of the other three cases. On the other hand, Case (a) yields higher cumulative water production than the other three cases. Figure 23 shows water saturation at the well blocks for each case. The results show that water saturation at the well blocks in Case (a) is higher than other three cases. The increase of water saturation increases the mobility of aqueous phase resulting in the increase of water production rate. It can be noticed that the shapes of water saturation curves and water production rate curves are consistent. On

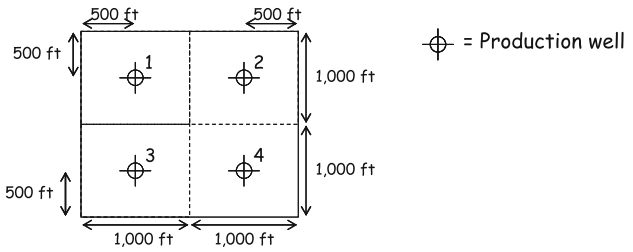

Fig. 18 Well structure in the methane hydrate used in this study

Table 5 Production schedule used in this study

Case	Starting time of operation (days)			
	Well no. 1 (t)	Well no. 2 (t)	Well no. 3 (t)	Well no. 4 (t)
a	0	0	0	0
b	0	90	90	180
c	0	60	60	180
d	0	90	90	0

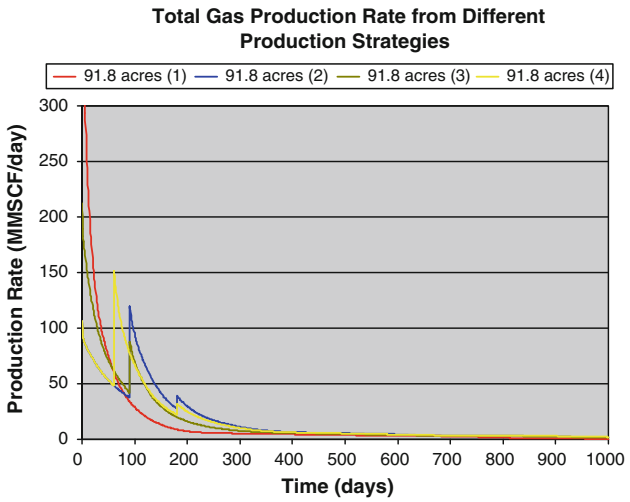

Fig. 19 Gas production rate—different production schedules scenario

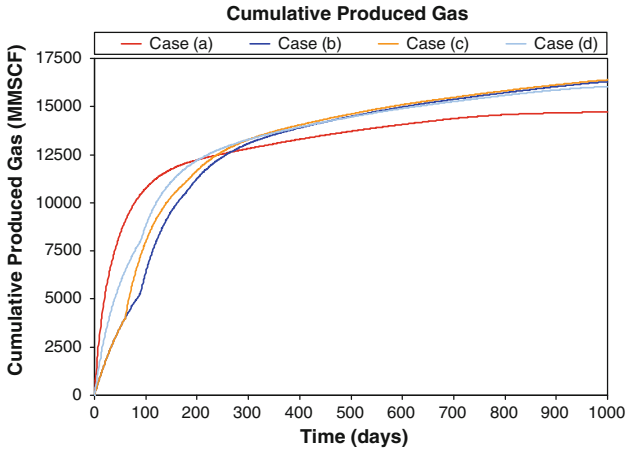

Fig. 20 Cumulative produced gas from different production schedules

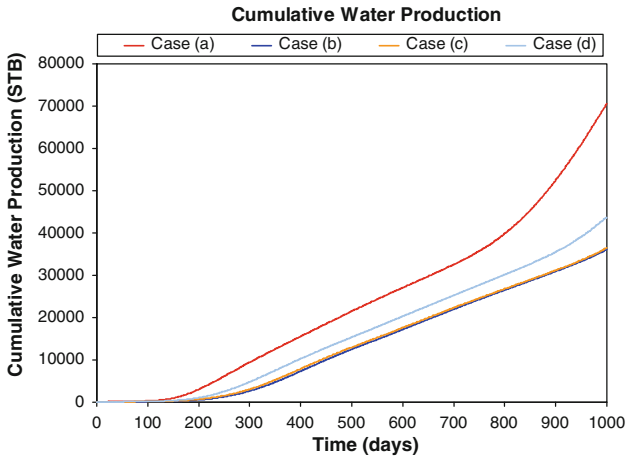

Fig. 21 Cumulative water production for different production schedule

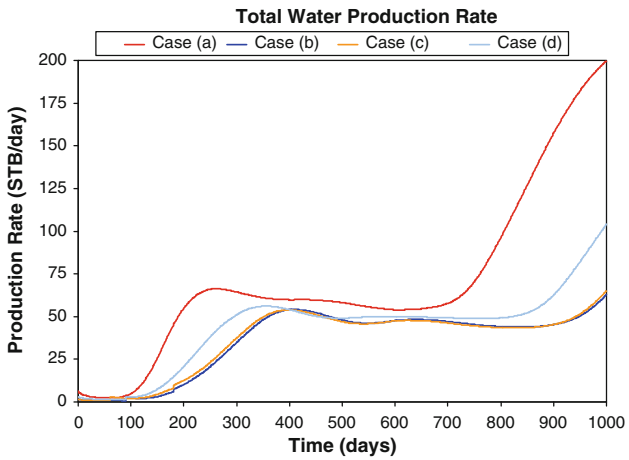

Fig. 22 Water production rate for different production schedule

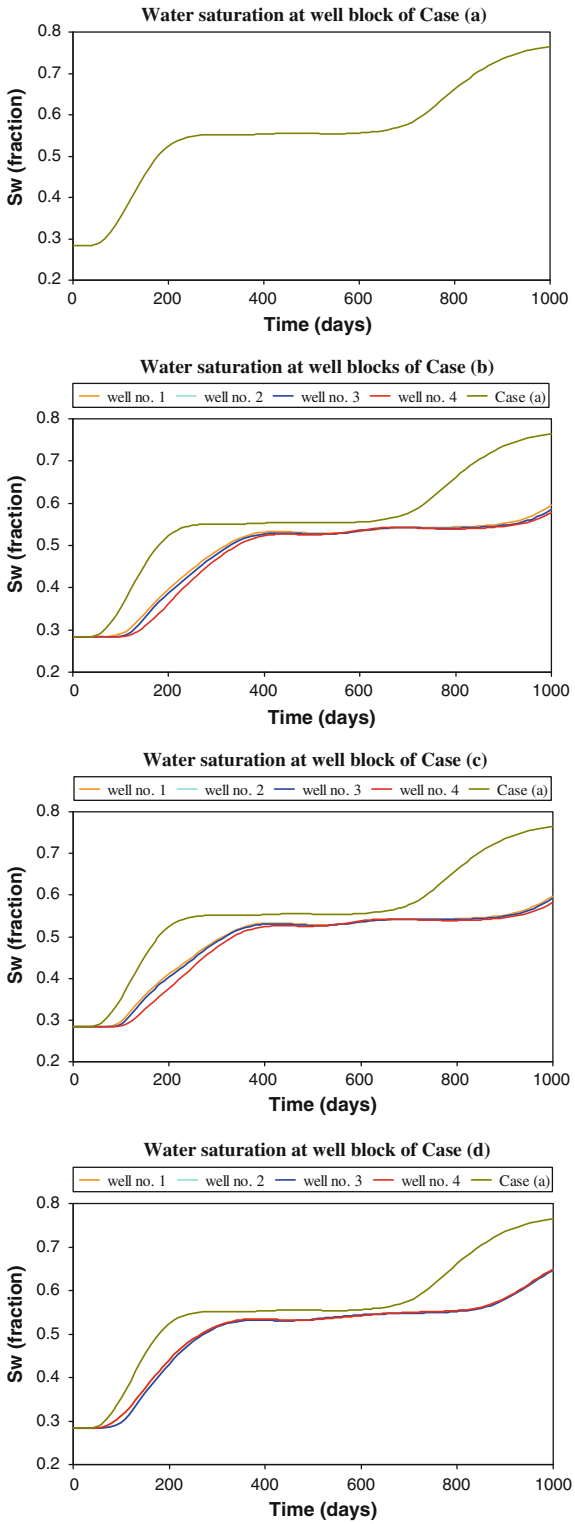

Fig. 23 Water saturation at well blocks for different production schedules

the other hand, the mobility of free-gas phase decreases due to the increase of water saturation resulting in the decrease of gas production rate. Accordingly, cumulative gas production of Case (a) is the lowest among the four

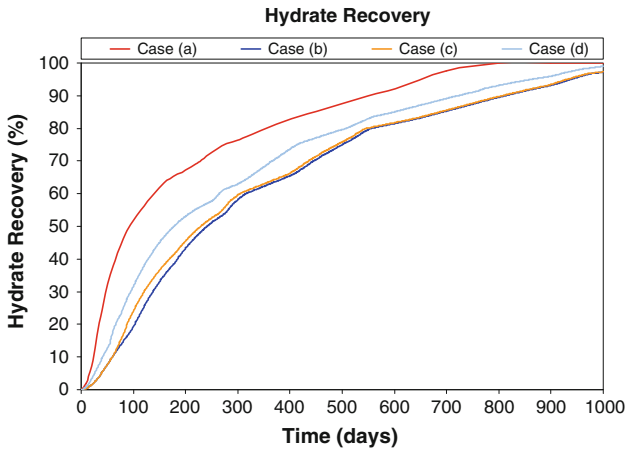

Fig. 24 Percent hydrate dissociation of different production schedules

cases; meanwhile cumulative water production of Case (a) is the highest.

Figure 24 shows the percent of methane-hydrate dissociations of the four production schedules. As expected, hydrate dissociation rates for Case (a) are faster than those of the other three cases. For example, it takes about 750 days for dissociating all hydrate phase in the system in Case (a), while it takes a bit longer than 1,000 days for dissociating all hydrate phase in the other three cases. This can be explained because all the wells are put on production at the very beginning of the production, and thus water saturations in Case (a) would increase more rapidly than in the other three cases. Faster hydrate dissociation provides faster released water rate from the dissociation process. Due to the gravitational effects, the released water (at the interface between hydrate and free-gas zone, inside the hydrate zone, and at the top of hydrate zone) flows to the lower part of the reservoir (free-gas zone) resulting in the increase of water saturation in free-gas zone. Meanwhile, released gas from dissociation inside and at the top of the hydrate zone does not flow to the well-completion zone. Consequently, water saturation in the free-gas zone increases with time. This indicates that faster hydrate dissociation does not always yield higher gas production. It depends on the locations of hydrate dissociation and well-completion zone.

According to Figs. 20 and 21, Case (c) yields the highest gas production efficiency. This case provides the highest gas production and lowest water production even though it dissociates less gas hydrate in the system than the other cases. The production efficiencies of Case (b) and (c) are not significantly different. Table 6 shows the comparison of the production performances of these four production schedules. Cumulative Gas to Water Ratio (CGWR) is the ratio of cumulative produced gas to cumulative produced water. It represents the amount of produced gas (MMSCF)

Table 6 Gas production for different production schedules

Case	Ratio		Amount	
	CGWR	% Improvement	Qg	% Improvement
a*	0.208	0.0	14,714	0.0
b	0.456	119.0	16,297	10.8
c	0.449	115.6	16,383	11.3
d	0.367	75.9	16,040	9.0

* Reference case

per 1 STB of cumulative produced water. Thus, the higher value of CGWR is preferred. The results show that cumulative gas production can be improved by putting the production wells at different times. Among the four cases examined in this study, Case (c) provides the best improvement of gas production. Cases (b) and (c) can provide substantial improvement of the CWGR ratio (more than 100% improvement). This simulation study shows that slowing hydrate dissociation rate by putting the wells on production at different times could improve gas production efficiency (when well completion is located only in the free-gas zone). However, it does not mean that slowing down hydrate dissociation rate by other means especially decreasing the number of production wells in the system will also improve gas production efficiency.

In the system shown in Fig. 18, all four wells are put on production for Case 1, but only wells no. 1 and 4 are put on production in Case 2. In both cases, however, production wells would start production at the same time (at $t = 0$). Figures 25 and 26 show percent methane-hydrate dissociation and cumulative gas production of these two cases, respectively. The results show that Case 2 provides lower dissociation rate and cumulative gas production than Case 1. The gas production efficiency in Case 2 does not improve even though the dissociation rate in Case 2 is lower than that in Case 1. This simulation results are consistent with the simulation results from the previous case study (effects of well spacing). The following conclusions could be drawn from this simulation exercise:

- In a multiple-well system, putting all wells on production at the different times yields lower hydrate dissociation rate than putting all wells on production at the same time.
- In a multiple-well system, gas production efficiency could be improved by putting wells on production at different times.

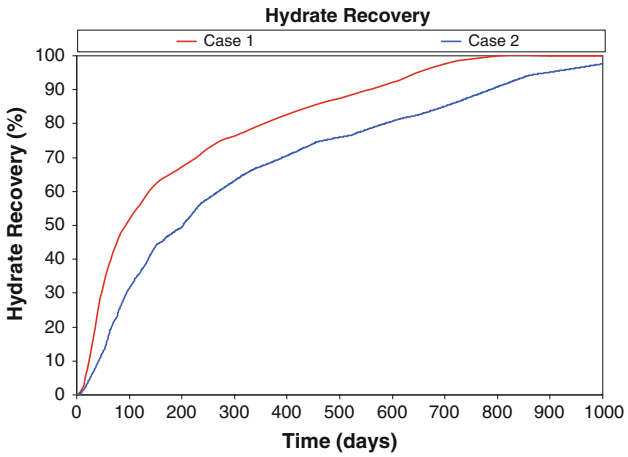

Fig. 25 Percent hydrate dissociation of the systems with different numbers of wells

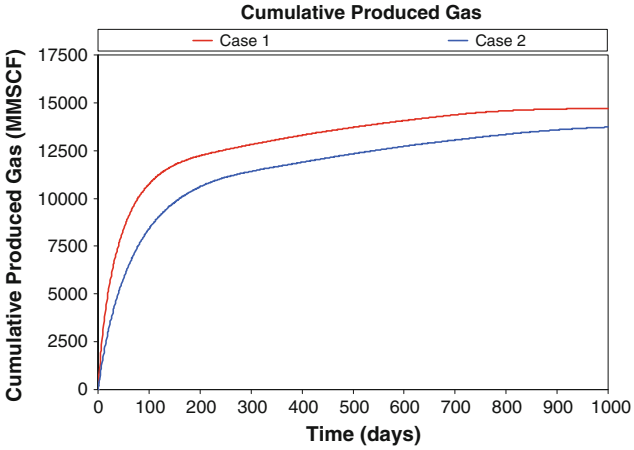

Fig. 26 Cumulative produced gas for different production schedules

Conclusion

A 3-dimensional, rectangular, compositional simulator for methane-hydrate system has been developed to examine the production characteristics from class 1 methane-hydrate reservoirs. In this study, a constant BHP (at 14.7 psia) is implemented as a production scheme for all simulation cases to explore the maximum production capacity of a given well. The effects of some production parameters on the production performances are also examined and the following conclusions can be drawn:

- The presence of gas hydrate on top of a conventional gas reservoir can dramatically improve gas productivity.
- For gas hydrate systems, gas production rate decreases with time; meanwhile water production rate increases with time (when a constant BHP is used as a production scheme).
- For class 1 hydrate reservoirs, completing a well only in the hydrate zone yields gas production much lower than completing a well in free gas zone.

- Moving well-completion location in relation to the movement of the interface between hydrate and free-gas zones can improve production efficiency.
- Smaller well-spacing system yields higher gas production. It does not show substantial improvement of gas productivity for the particular system used in this study. However, the percent improvement values could change depending upon the rock and fluid properties and reservoir structure.
- In a multiple well system, putting all wells on production at different time yields better production efficiency (it yields higher gas production and less water production).

References

Boswell R, Shelander D, Lee M, Latham T, Collett T, Guerin G, Moridis G, Reagan M, Goldberg D (2009) Occurrence of gas hydrate in Oligocene Frio sand: Alaminos Canyon Block 818: Northern Gulf of Mexico. J Marine Petrol Geol 26(8):1499–1512

Burshears M, O'Brien T, and Malone R (1986), A multi-phase, multi-dimensional, variable composition simulation of gas production from a conventional gas reservoir in contact with hydrates, SPE paper 15246 presented at the SPE Unconventional Gas Technology Symposium, May 18–21, Louisville, Kentucky

Holder G, and Angert P (1982) Simulation of gas production from a reservoir containing both gas hydrates and free natural gas, SPE Paper 11105 presented at the 57th Annual Technical Conference and Exhibition, Sept. 26–29, New Orleans, LA

Lee AL, Gonzalez MH, Eakin BE (1966) "Viscosity of natural gases". J Pet Tech 18(8):997–1000

Mahajan D, Taylor CE, and Mansoori GA (eds), (2007) Natural gas hydrate/clathrate. J Petrol Sci Eng 56(1–3)

Makogon YF, Holditch SA, Makogon TY (2007) Natural gas-hydrates—a potential energy source for the 21st Century. J Petrol Sci Eng 56(1–3):14–31

Moridis GJ (2003) Numerical studies of gas production from methane hydrates. SPE J 8(4):359–370

Moridis GJ and Collett TS (2003), "Strategies for gas production from hydrate accumulations under various geologic conditions", Report LBNL-52568, Lawrence Berkeley National Laboratory, Berkeley, California

Moridis GJ, Seol Y and Kneafsey T (2005) "Studies of reaction kinetics of methane hydrate dissociation in porous media", Paper 1004, Proceedings of the 5th International Conference on Gas Hydrates, Trondheim, Norway, June 13–16, 21–30 (LBNL-57298)

Moridis GJ, Kowalsky MB, Pruess K (2007) Depressurization-induced gas production from Class-1 hydrate deposits. SPE J Res Eval Eng 10(5):458–481

Moridis GJ, Kowalsky M and Pruess K (2008) TOUGH + HYDRATE v1.0 User's Manual: a code for the simulation of system behavior in hydrate-bearing geologic media, LBNL-00149E

Moridis GJ, Collett TS, Boswell R, Kurihara M, Reagan MT, Koh C, Sloan ED (2009) Toward production from gas hydrates: current status, assessment of resources, and simulation-based evaluation of technology and potential. SPE Res Eval Eng 12(5):745–771

Moridis GJ, Collett TS, Pooladi-Darvish M, Hancock S, Santamarina C, Boswell R, Kneafsey T, Rutqvist J, Kowalsky M, Reagan MT, Sloan ED, Sum AK, Koh C (2011) "Challenges, uncertainties and issues facing gas production from gas hydrate deposits". SPE Res Eval Eng 14(1):76–112

Peaceman DW (1983) Interpretation of wellblock pressures in numerical reservoir simulation with nonsquare gridblocks and anisotropic permeability, SPE Paper 10528. SPE J. 23(3):531–543

Peng DY, Robinson DB (1976) A new two-constant equation of state. Ind Eng Chem Fundam 15(1):59–64

Perry RH and Green DW (ed), 1997, Perry's chemical engineers' handbook, 7th edn. Mc-Graw Hill, New York

Pooladi-Darvish M (2004) Gas production from hydrate reservoirs and its modeling. J Petrol Technol 56(6):65–71

Silpngarmlert S, Ertekin T, and Ayala L (2012) Numerical modeling of gas production from methane hydrate reservoirs by depressurization. Int J Model Simul (in press)

Somerton WH et al. (1973) "Thermal behavior of unconsolidated oil sands", SPE Paper 4506, 48th Annual Fall Meeting of the Society of Petroleum Engineers, Las Vegas, NV

Sun X, Nanchary N, Mohanty KK (2005) *1*-D modeling of hydrate depressurization in porous media. Transp Porous Med 58(3): 315–338

Verma A, Pruess K, Tsang CF, and Witerspoon PA (1985) "A study of two-phase concurrent flow of steam and water in an unconsolidated porous medium", Proceedings of the 23rd National Heat Transfer Conference. Am Soc Mech Eng, Denver, CO, p. 135–143